POLITECNICO
MILANO 1863

SCUOLA DI INGEGNERIA INDUSTRIALE
E DELL'INFORMAZIONE

Executive Summary of the Thesis

Integrated Aerodynamic and Biomechanical Analysis of Paralympic Tandem Time-Trial Cycling

Laurea Magistrale in Aeronautical Engineering - Ingegneria Aeronautica

Author: Giovanni Restelli

Advisor: Prof. Claudio Somaschini

Co-advisor: Marta Gandolla

Academic year: 2024-2025

1. Introduction

Paralympic tandem time-trial cycling involves two athletes operating as a single mechanically and aerodynamically coupled system. Unlike single-rider cycling, aerodynamic performance in tandem configurations cannot be interpreted as the sum of two independent riders. The rear athlete operates within the wake generated by the pilot, and the resulting shielding effects, altered pressure recovery, and recirculation structures in the inter-rider region produce a system-dependent aerodynamic response. [1, 4] Consequently, posture optimisation must be addressed at system level rather than through independent rider adjustments.

At the same time, aerodynamic posture refinement must remain physically adoptable by the athletes on the existing tandem platform and sustainable under race conditions. The problem addressed here is therefore not limited to drag minimisation, as the influence of upper-body posture on aerodynamic drag has been widely documented in single-rider time-trial cycling [3]. It is necessary to determine whether aerodynamically favourable configurations introduce measurable biomechanical consequences in terms of joint kinematics, muscle activation patterns, or fatigue development.

At elite racing speeds, aerodynamic drag represents the dominant external resistance, typically accounting for more than 85% of total resistive forces [1]. The drag force can be expressed as

$$F_D = \frac{1}{2}\rho v^2 C_d A \tag{1}$$

where ρ is air density, v is the relative airflow velocity, and C_dA is the effective drag area. Because aerodynamic power scales with v^3, even small reductions in C_dA can translate into measurable time savings over race distance, especially in elite-level competition, where marginal aerodynamic gains may determine podium outcomes.

The central objective of this investigation is to evaluate aerodynamic performance and biomechanical response within a unified framework, combining Computational Fluid Dynamics (CFD) simulations with motion capture, surface electromyography (EMG), and musculoskeletal modelling in order to quantify whether aerodynamically optimised configurations remain neuromuscularly sustainable under controlled high-intensity conditions.

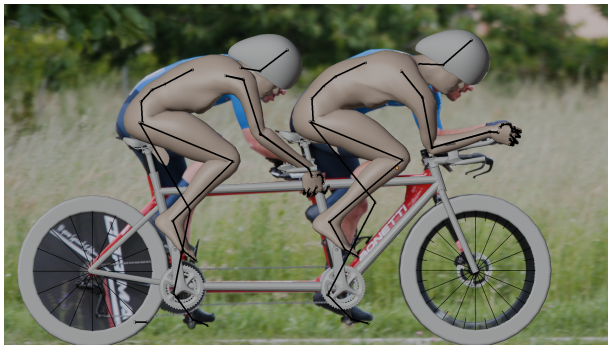

Figure 1: 3D model photographical comparison

2. Objectives and Scope

The study aims to:

- quantify macroscopic posture-dependent variations in aerodynamic performance across multiple realistic configurations;
- analyse wake interaction mechanisms between pilot and stoker;
- evaluate joint kinematics, muscle activation patterns, and fatigue indicators under controlled laboratory conditions;
- assess the reliability and limitations of optimisation-based musculoskeletal modelling in aggressive time-trial postures;
- identify potential trade-offs between aerodynamic efficiency and neuromuscular sustainability.

The analysis is grounded on data acquired from two elite World Champion athletes and focuses on configurations that are realistically adoptable in training and competition.

Aerodynamic and biomechanical analyses are performed on identical rider configurations, ensuring direct comparability between fluid-dynamic and neuromuscular responses.

3. Methodology

3.1. Aerodynamic Modelling

Seven tandem configurations, complemented by two pilot-only reference cases (baseline and lowered head position), were reconstructed through anthropometric digital modelling of the athletes combined with detailed CAD representation of the tandem bicycle (Figures 1-2). The analysed variations include pilot head position, inter-rider longitudinal spacing, and stoker cockpit geometry.

All simulations were performed using Open-

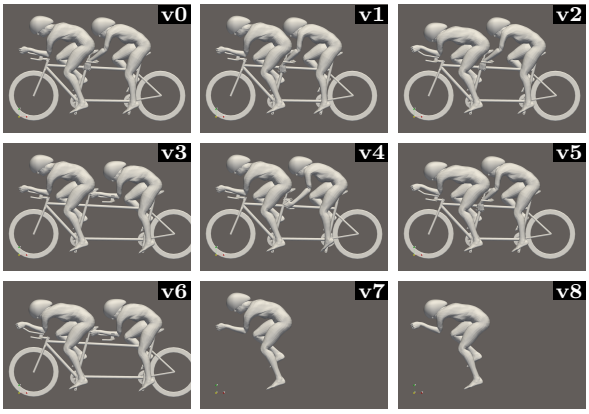

Figure 2: Three-dimensional CAD models of the nine analysed configurations (v0–v8).

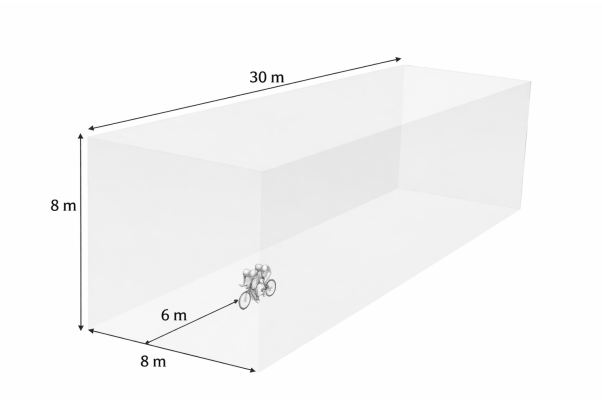

Figure 3: Simulation domain representation with dimensions.

FOAM v2406 under steady Reynolds-Averaged Navier–Stokes (RANS) formulation. The computational domain, represented in Figure 3, was sized to ensure negligible blockage effects (below 0.5%), and mesh independence was verified through systematic refinement studies. Local volumetric refinement was applied in the interaction region between pilot and stoker and in the near-wake development zone.

As the objective of the study is to isolate the effects of torso positioning, periodic leg motion and wheel rotation were neglected, together with secondary geometric details such as wheel spokes.

Aerodynamic performance was evaluated through:

- global C_dA comparison across configurations;
- cumulative drag distributions along streamwise and vertical directions;
- qualitative flow-field analysis.

3.2. Biomechanical Assessment

The biomechanical analysis was designed to evaluate whether posture variations associated with aerodynamic optimisation modify joint kinematics, muscle activation strategies, or fatigue development under controlled mechanical conditions.

The logical workflow consists of three interconnected stages as represented in Figure 4. First, full-body kinematics and surface electromyographic activity were recorded during steady-state cycling in different rider positions. Second, the measured kinematics were reconstructed and implemented within a musculoskeletal model to evaluate joint angles and estimate muscle activation patterns through inverse dynamics. Third, EMG data were processed to quantify posture-dependent differences in muscle recruitment and to assess fatigue-related indicators. Finally, experimentally measured EMG activity was compared with model-predicted activations to evaluate consistency and identify limitations of optimisation-based simulations.

Biomechanical evaluation was conducted through full-body inertial motion capture (Xsens), surface electromyography (Delsys Trigno), and musculoskeletal modelling in the AnyBody Modeling System.

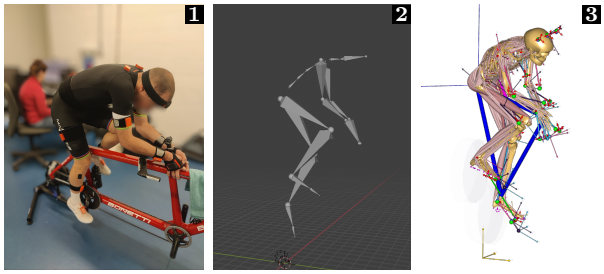

Figure 4: Biomechanical workflow: (1) motion capture and EMG acquisition; (2) BVH reconstruction; (3) musculoskeletal simulation in the AnyBody Modeling System.

Experimental trials were performed on the stoker in three rider positions: Road (standard handlebar, corresponding to configuration v4), Frame-clench (compact posture gripping the frame, corresponding to configurations v0, v1, v2 and v5), and Time-trial (aerobar posture, corresponding to configurations v3 and v6). Tests were conducted under steady-state cycling at four combinations of cadence (80 and 100 rpm) and power (150 and 300 W), resulting in 12 trials. Kinematic analysis, EMG–model comparison, and fatigue indicators were evaluated on the 5-minute steady-state trial at 300 W and 100 rpm, while cycle-averaged EMG activation patterns were examined across all four cadence–power combinations.

Fatigue-related indicators were quantified using frequency-domain EMG metrics (median frequency and mean frequency) and RMS amplitude analysis. A progressive shift of the EMG power spectrum toward lower frequencies is commonly interpreted as a marker of developing neuromuscular fatigue [2]. Surface EMG signals were recorded from the soleus (SOL), tibialis anterior (TA), rectus femoris (RF), and semitendinosus (ST).

4. Aerodynamic Results

4.1. Global Aerodynamic Performance

The global aerodynamic performance of the nine configurations was quantified in terms of effective drag area C_dA. Table 1 summarises the geometric variations introduced across the tested cases.

As reported in Table 2, the global drag area across tandem configurations (v0–v6) ranges from 0.251 to 0.271 m^2. Relative to the baseline configuration v0 (0.265 m^2), the best-performing case (v5, 0.251 m^2) achieves a drag reduction of 5.3%.

Configuration v5 exhibits the lowest global C_dA (0.251 m^2), while v4 shows the highest value (0.271 m^2). The bicycle contribution remains nearly constant across cases (0.059–0.062 m^2), indicating that the observed spread in drag is predominantly associated with rider posture and pilot–stoker aerodynamic coupling.

Pilot-only reference cases (v7–v8) were introduced to isolate the intrinsic aerodynamic effect of pilot posture from the interaction with the stoker. Lowering the pilot head reduces the isolated pilot drag from 0.131 m^2 to 0.113 m^2, corresponding to a reduction of 14%. This confirms that the head-lowered position provides a genuine aerodynamic benefit independently of tandem wake-coupling effects.

Table 1: Summary of analysed configurations. v7 and v8 are pilot-only configurations used to isolate the effect of pilot posture variation. Δx is the inter-rider distance. FC is Frame-clench position, in which the stoker grips to the frame, TT is Time-trial position with aerobars, while Road is a classic position with road handlebar.

Cfg	Pilot	Stoker	Δx
v0	Baseline	FC	0
v1	Baseline	FC	-7 cm
v2	Lower head	FC	0
v3	Baseline	TT	$+20$ cm
v4	Baseline	Road	0
v5	Lower head	FC	-7 cm
v6	Lower head	TT	$+20$ cm
v7	Baseline	–	–
v8	Lower head	–	–

Table 2: Aerodynamic drag area C_dA (average over the last 500 iterations). All values are expressed in m^2.

Cfg	Global	Bike	Pilot	Stoker
v0	0.265	0.062	0.094	0.109
v1	0.256	0.060	0.099	0.097
v2	0.258	0.061	0.091	0.106
v3	0.264	0.061	0.100	0.103
v4	0.271	0.059	0.099	0.113
v5	0.251	0.059	0.093	0.099
v6	0.255	0.060	0.101	0.095
v7	0.131	—	0.131	—
v8	0.113	—	0.113	—

4.2. Wake Interaction and Non-Additive Effects

Flow-field visualisation provides further insight into the mechanisms underlying the measured drag variations.

The surface total pressure coefficient maps (Figure 5) show how variations in pilot posture and inter-rider spacing modify the pressure distribution in the transition region between the two athletes.

Changes in spacing alter the extent and continuity of the high-pressure zone over the pilot back and the subsequent pressure field impinging on the stoker upper body. These variations are consistent with the measured differences in global drag.

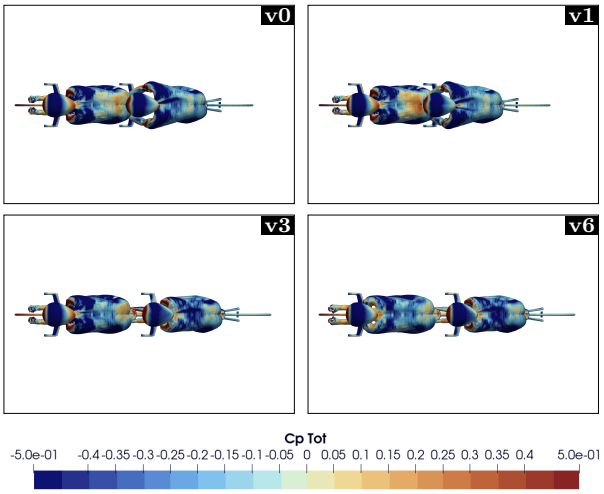

Figure 5: Surface total pressure coefficient ($C_{p,tot}$) distribution for selected configurations (v0, v1, v3, v6). The colour scale is identical for all cases.

The isosurface visualisations at $C_{p,tot} = -0.1$ (Figure 6) provide qualitative insight into wake development in the inter-rider region. Although the differences are subtle, variations in spacing and pilot alignment modify the continuity and spatial extent of the low-pressure region between the two riders.

Reduced spacing tends to produce a more merged wake structure, while increased longitudinal distance promotes a slightly more extended separation between the two flow structures.

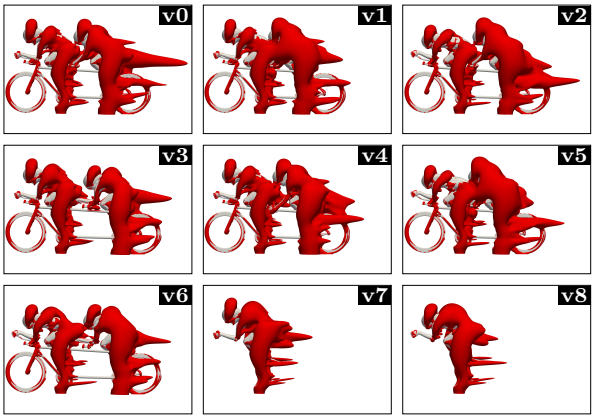

Figure 6: Isosurface visualisation at $C_{p,tot} = -0.1$ for configurations v0–v8.

Overall, the visualisations support quantitative results, indicating that variations in spacing and pilot posture reshape the wake structure and contribute to observed differences in global drag. Importantly, the aerodynamic behaviour is in-

herently non-additive. Improvements observed in isolated pilot simulations (v7–v8) do not translate linearly to tandem configurations. The stoker rides within the disturbed flow generated by the pilot, and the aerodynamic response of the system depends on how this wake develops in the inter-rider region. Consequently:

- reduced spacing increases shielding of the stoker but modifies the pressure recovery behind the pilot;
- increased longitudinal distance exposes a larger portion of the stoker to the freestream flow, but allows the stoker to assume a more streamlined position;
- combined changes in pilot posture and spacing alter the wake structure and lead to non-additive variations in global drag.

A configuration-wise comparison further clarifies these interaction effects.

Lowering the pilot head while keeping spacing constant (v0–v2) reduces global C_dA from 0.265 to 0.258 m^2, confirming the aerodynamic benefit of improved upper-body alignment even in the presence of wake coupling. When head lowering is combined with reduced spacing (v1-v5), the drag decreases more markedly from 0.256 to 0.251 m^2, indicating a constructive interaction between improved pilot alignment and enhanced stoker shielding.

Similarly, in the rearward stoker configurations (v3–v6), lowering the pilot head reduces C_dA from 0.264 to 0.255 m^2, showing that the aerodynamic advantage of pilot alignment persists despite increased inter-rider separation.

Conversely, adopting a conventional road handlebar for the stoker (v4) results in the highest drag (0.271 m^2), highlighting the aerodynamic penalty associated with a less compact upper-body posture in the rear position.

These observations reinforce the need for a coupled analysis framework in which pilot and stoker configurations are evaluated simultaneously.

5. Biomechanical Results

5.1. Kinematic Consistency

Joint kinematic analysis focused on hip, knee, and ankle angles throughout the pedal cycle. The adopted joint angle conventions are illustrated in Figure 7, while Tables 3 and 4 summarise the corresponding kinematic results. Despite substantial variations in upper-body posture across configurations, lower-limb kinematics remained remarkably stable.

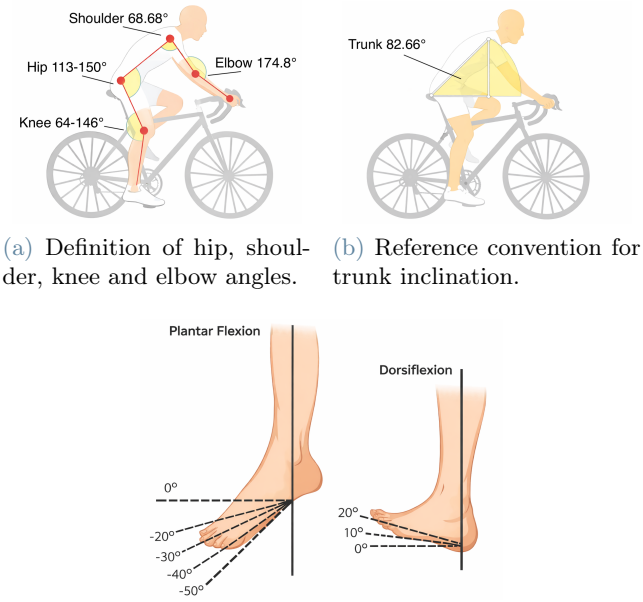

(a) Definition of hip, shoulder, knee and elbow angles.

(b) Reference convention for trunk inclination.

(c) Definition of ankle plantar angle.

Figure 7: Kinematic angle conventions adopted for upper- and lower-limb analysis. All joint angles are defined according to the anatomical reference frames implemented in the motion capture processing workflow.

Table 3: Mean upper-body joint angles (mean ± standard deviation, in degrees)

Angle [deg]	Road	FC	TT
Trunk	82.66±1.15	71.17±1.17	73.90±1.24
Shoulder	68.68±1.85	84.42±2.36	93.39±1.59
Elbow	174.80±1.32	143.29±2.42	104.23±1.33

Table 4: Lower-limb joint range of motion across riding positions (mean ± standard deviation, in degrees)

Joint	Side	Road	FC	TT
Hip	R	36.98 ± 0.25	39.45 ± 0.32	37.13 ± 0.86
	L	41.07 ± 0.49	42.57 ± 0.57	42.13 ± 1.20
Knee	R	82.09 ± 0.80	84.18 ± 0.75	78.38 ± 0.89
	L	76.06 ± 0.75	82.96 ± 0.72	73.37 ± 0.10
Ankle	R	58.46 ± 1.87	61.36 ± 1.87	57.37 ± 2.01
	L	59.78 ± 1.13	60.70 ± 1.13	57.71 ± 1.74

Across all configurations, hip, knee, and ankle ROM values remain within comparable ranges, indicating that pedalling mechanics are primarily constrained by bicycle geometry rather than upper-body posture adjustments.

5.2. Muscle Activation and Fatigue Indicators

Cycle-averaged EMG analysis revealed consistent activation timing across configurations (Figure 8). EMG profiles remained temporally stable during the steady-state trial, with limited cycle-to-cycle variability. Differences between positions were generally modest, with no substantial shifts in activation phase.

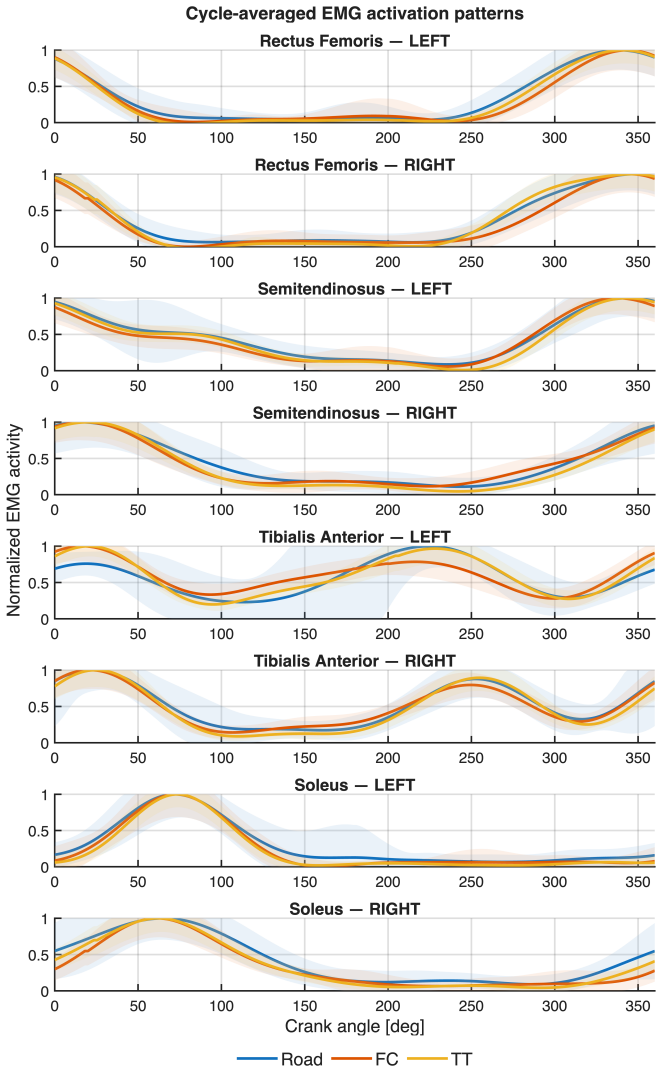

Figure 8: Comparison of cycle-averaged EMG activation patterns between road, frame-clench and time-trial positions under identical mechanical conditions. EMG amplitude is normalised and is presented along its standard deviation.

The muscle activation patterns predicted by the AnyBody musculoskeletal model did not provide quantitatively consistent or practically comparable results with respect to the experimentally measured EMG signals. These findings suggest that musculoskeletal simulations based on generic recruitment criteria may not fully capture the task-specific neuromuscular strategies adopted by elite athletes under high-intensity conditions, where selective co-contractions and intentional load redistribution can deviate from the assumption of minimising maximum relative activation.

The focus was subsequently shifted from activation patterns to fatigue development. As reported in Table 5, no configuration emerged as globally superior in fatigue mitigation. Rather, posture changes redistributed neuromuscular demand across muscle groups without consistently increasing fatigue under steady-state high-intensity conditions.

Table 5: MF slope (5 min, 300 W). Negative values are associated with a shift toward lower frequency components and are commonly interpreted as indicative of neuromuscular fatigue.

Muscle	Road	FC	TT
TA-R	-0.1525	-0.0846	0.0190
TA-L	-0.1723	0.0200	-0.0190
ST-R	0.0032	0.0075	0.0141
ST-L	-0.1600	-0.0142	-0.0614
RF-R	-0.0150	0.0406	-0.0795
RF-L	-0.0710	-0.1422	-0.0803
SOL-R	-0.0421	-0.0503	-0.0240
SOL-L	-0.0492	0.0023	-0.0239

6. Conclusions

This work presented an integrated experimental–numerical investigation of performance optimisation in Paralympic tandem time-trial cycling, combining steady RANS CFD simulations with motion capture, surface EMG analysis, and musculoskeletal modelling applied to identical rider configurations.

From an aerodynamic perspective, the analysed tandem configurations produced a global C_dA reduction of 5.3% relative to the baseline configuration v0, decreasing from 0.265 to 0.251 m^2. The lowest drag configuration (v5) resulted from the combined effect of pilot head lowering and

reduced inter-rider spacing. Pilot-only reference simulations showed a reduction from 0.131 to 0.113 m^2 when lowering the head position (14%), confirming the strong sensitivity of the system to upper-body alignment. Flow-field visualisations demonstrated that variations in inter-rider distance and pilot posture reshape the wake structure in the transition region, leading to inherently non-additive drag behaviour.

From a biomechanical perspective, lower-limb joint kinematics remained consistent across configurations, with comparable hip, knee, and ankle ranges of motion. Fatigue analysis over the 5-minute steady-state trial did not reveal systematic amplification of neuromuscular fatigue in aerodynamically refined positions. Instead, posture modifications redistributed muscular demand across muscle groups without inducing critical penalties.

A relevant methodological outcome concerns musculoskeletal modelling. Optimisation-based inverse-dynamics simulations did not quantitatively reproduce experimentally measured EMG activation patterns. This suggests that musculoskeletal simulations relying on generic recruitment criteria may not fully capture the task-specific neuromuscular strategies adopted by elite athletes under high-intensity conditions, reinforcing the need for experimental validation when interpreting model predictions.

Overall, the results indicate that realistic aerodynamic improvements can be achieved within the tested configurations without compromising neuromuscular sustainability. Notably, the configuration associated with the lowest aerodynamic drag does not exhibit signs of premature fatigue under high-intensity conditions, suggesting that aerodynamic optimisation does not inherently impose a physiological penalty.

At the same time, posture modifications produce measurable changes in muscle fatigue distribution, implying that aerodynamically refined positions require specific neuromuscular adaptation. From a practical perspective, this highlights the importance of position-specific training and progressive familiarisation with aggressive configurations to ensure sustainable performance in competition.

More broadly, the combined aerodynamic–biomechanical evaluation provides actionable guidance for tandem setup design: the optimal configuration cannot be selected based on drag reduction alone, but must account for rider interaction, muscular redistribution, and long-term feasibility. This integrated perspective is essential for translating engineering optimisation into real competitive advantage.

Future developments should include wind-tunnel validation of the numerical aerodynamic results, extension of the experimental protocol to a larger athlete cohort, longer-duration trials to investigate fatigue accumulation, open-field testing combining power-meter data, aerodynamic field methods and fatigue monitoring, and a systematic parametric exploration of rider positioning variables. Such extensions would enable the development of a more generalised and experimentally validated optimisation framework.

7. Acknowledgements

I sincerely thank Federico Andreoli, 2025 Paralympic Road World Champion, for his trust, commitment, and availability throughout the experimental campaign.

Ethical Compliance

All experimental procedures were conducted in accordance with the ethical standards of Politecnico di Milano and complied with regulations governing research involving human participants. Written informed consent was obtained from the participant prior to data collection.

References

[1] B. et al. Blocken. Cfd simulation of cyclist aerodynamics. *Journal of Wind Engineering*, 2013.

[2] C. J. De Luca. Myoelectrical manifestations of localized muscular fatigue in humans. *Critical Reviews in Biomedical Engineering*, 11(4):251–279, 1984.

[3] D. M. Fintelman, M. Sterling, H. Hemida, and F.-X. Li. Optimal cycling time trial position models: A comparison between cfd and field testing. *Journal of Biomechanics*, 47(9):2084–2090, 2014.

[4] P. et al. Mannion. Aerodynamic investigation of tandem cycling configurations. *Journal of Wind Engineering and Industrial Aerodynamics*, 2018.